Disruption of angiogenesis and tumor growth with an orally active drug that stabilizes the inactive state of PDGFRβ/B-RAF

Eric A. Murphy[a], David J. Shields[a], Konstantin Stoletov[a], Elena Dneprovskaia[b], Michele McElroy[c], Joshua I. Greenberg[c], Jeff Lindquist[a], Lisette M. Acevedo[a], Sudarshan Anand[a], Bharat Kumar Majeti[a], Igor Tsigelny[d], Adrian Saldanha[e], Breda Walsh[a], Robert M. Hoffman[c,f], Michael Bouvet[c], Richard L. Klemke[a], Peter K. Vogt[g], Lee Arnold[h], Wolfgang Wrasidlo[a], and David A. Cheresh[a,1]

[a]Department of Pathology, Moores Cancer Center, University of California, San Diego, La Jolla, CA 92093; [b]TargeGen Inc., San Diego, CA 92121; [c]Department of Surgery, Moores Cancer Center, University of California, San Diego, La Jolla, CA 92093; [d]Department of Neurosciences, University of California, San Diego, La Jolla, CA 92093; [e]Department of Chemistry and Biochemistry, University of California, San Diego, La Jolla, CA 92093; [f]Anticancer Inc., San Diego, CA 92111; [g]Department of Molecular and Experimental Medicine, The Scripps Research Institute, La Jolla, CA 92037; and [h]Kinagen Inc., Encinitas, CA 92024

Edited* by Tony Hunter, The Salk Institute for Biological Studies, La Jolla, CA, and approved December 31, 2009 (received for review August 19, 2009)

Kinases are known to regulate fundamental processes in cancer including tumor proliferation, metastasis, neovascularization, and chemoresistance. Accordingly, kinase inhibitors have been a major focus of drug development, and several kinase inhibitors are now approved for various cancer indications. Typically, kinase inhibitors are selected via high-throughput screening using catalytic kinase domains at low ATP concentration, and this process often yields ATP mimetics that lack specificity and/or function poorly in cells where ATP levels are high. Molecules targeting the allosteric site in the inactive kinase conformation (type II inhibitors) provide an alternative for developing selective inhibitors that are physiologically active. By applying a rational design approach using a constrained amino-triazole scaffold predicted to stabilize kinases in the inactive state, we generated a series of selective type II inhibitors of PDGFRβ and B-RAF, important targets for pericyte recruitment and endothelial cell survival, respectively. These molecules were designed in silico and screened for antivascular activity in both cell-based models and a Tg (*fli1-EGFP*) zebrafish embryogenesis model. Dual inhibition of PDGFRβ and B-RAF cellular signaling demonstrated synergistic antiangiogenic activity in both zebrafish and murine models of angiogenesis, and a combination of previously characterized PDGFRβ and RAF inhibitors validated the synergy. Our lead compound was selected as an orally active molecule with favorable pharmacokinetic properties which demonstrated target inhibition in vivo leading to suppression of murine orthotopic tumors in both the kidney and pancreas.

type II inhibitor | kinase inhibition | pancreatic carcinoma | pericyte | cell-based screening

RAF is an important convergent point downstream of FGFR and VEGFR2 signaling in endothelial cells and has previously been shown to play a critical role in endothelial cell survival during angiogenesis (1–3). PDGFRβ is a receptor tyrosine kinase that is essential for promoting proper pericyte function, which stabilizes blood vessels and enables vessel maturation (4–6). We rationalized that inhibition of both RAF and PDGFRβ would produce a potent antiangiogenic effect by targeting the two primary cell types involved in angiogenesis and vascular remodeling, endothelial cells and pericytes, respectively. As such, we designed compounds predicted to inhibit both RAF and PDGFRβ in a selective manner.

The recent approval of imatinib (7, 8) (**1**) and sorafenib (9) (**2**), inhibitors which target PDGFRβ (10) and/or B-RAF (11, 12), has created much enthusiasm for small molecules that stabilize the inactive kinase conformation (13–15). These two molecules were cocrystallized with their respective targets, B-RAF (16) and Abl (17) kinase domains, and shown to interact in part with the allosteric site in the "DFG-out" conformation, referred to as type II inhibition. Based on the binding mode of sorafenib and imatinib, we synthesized an amino-triazole scaffold designed to target the allosteric site of both PDGFRβ and B-RAF using a combination of in silico screening and in vitro bioassays. Here we report the discovery of a selective PDGFRβ/RAF type II inhibitor, termed **6**. Importantly, as predicted, this molecule does not inhibit activated kinases in vitro and thus would be overlooked in high-throughput screening applications. Dual inhibition of PDGFRβ/RAF activity produces a potent antiangiogenic effect in both zebrafish and murine models of angiogenesis that is not seen with the inhibition of either target alone. Combination of separate inhibitors of PDGFRβ and RAF reproduces the antiangiogenic effects of compound **6** in both the zebrafish in vivo and a pericyte/endothelial cell tube formation assay in vitro, and further validates the dual targeting of PDGFRβ and RAF as a synergistic approach. Additionally, **6** suppresses tumor growth in orthotopic tumor models of pancreatic and renal cell carcinoma.

Results

Design of a Selective Type II PDGFRβ/B-RAF Inhibitor. Whereas the overall homology of the PDGFRβ and B-RAF kinase domains is relatively low (29.1% homology and 47.3% similarity; Fig. S1*A*), these two kinases feature structurally related type II pockets, guiding the design of an amino-triazole scaffold which could generally fit into the allosteric site in the inactive conformation of these and other kinases while avoiding the ATP pocket (Fig. 1*A*). Further details of the docking studies are described in *SI Results* and Fig. S1*B*. Amino-triazole-based compounds were screened in human primary-cell-based assays for their ability to suppress PDGF-BB-mediated PDGFRβ autophosphorylation in vascular smooth muscle cells (VSMCs) and growth-factor-mediated MEK and ERK phosphorylation in endothelial cells (ECs) (Fig. 1 *B* and *C*). Structure–activity relationships (SARs) demonstrate the critical substituents for cell-based PDGFRβ and RAF inhibition (Fig. 1*D*) and are further described in *SI Results*. Active compounds were then screened for antiangiogenic activity in the developing zebrafish (from 20 to 48 h postfertilization; hpf) by evaluating the growth of intersegmental vessels. Successive rounds of molecular modeling, chemical synthesis, and cell-based and zebrafish screening were performed to refine the active molecules.

Author contributions: E.A.M., D.J.S., M.B., W.W., and D.A.C. designed research; E.A.M., D.J.S., K.S., E.D., M.M., J.I.G., J.L., L.M.A., S.A., B.K.M., I.T., A.S., and B.W. performed research; E.A.M., D.J.S., J.I.G., R.M.H., R.L.K., P.K.V., L.A., W.W., and D.A.C. analyzed data; and E.A.M. and D.A.C. wrote the paper.

The authors declare no conflict of interest.

*This Direct Submission article had a prearranged editor.

[1]To whom correspondence should be addressed. E-mail: dcheresh@ucsd.edu.

This article contains supporting information online at www.pnas.org/cgi/content/full/0909299107/DCSupplemental.

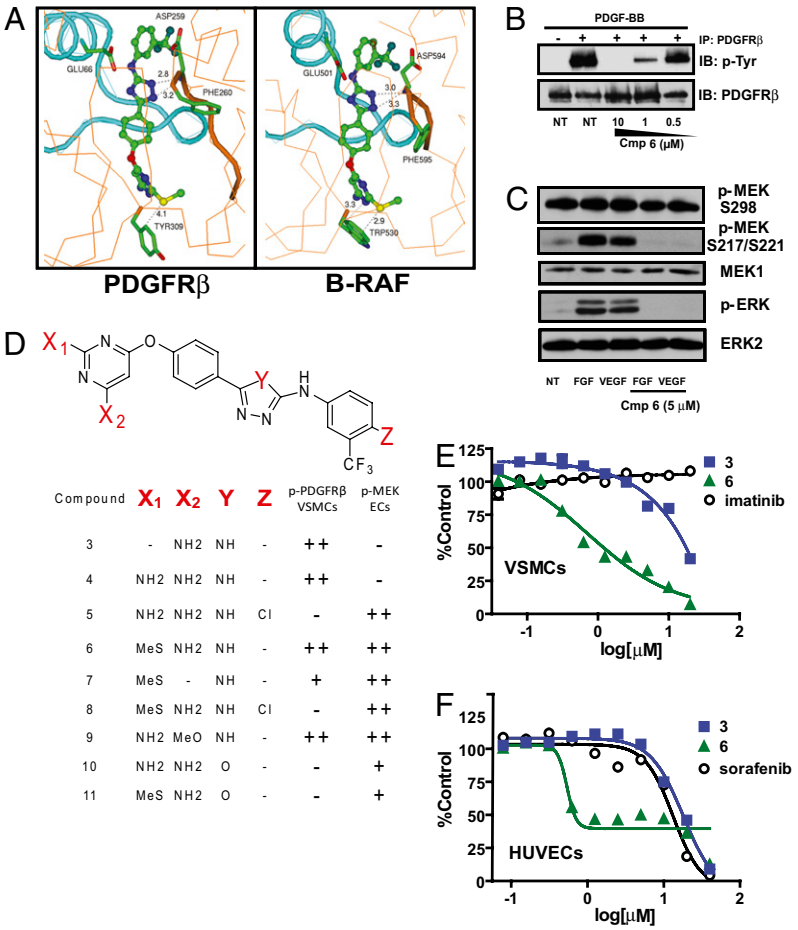

Fig. 1. Dual targeting of PDGFRβ and B-RAF. (*A*) Molecular modeling of the amino-triazole-based small molecules in PDGFRβ and B-RAF, respectively. The crystal structure of B-RAF [Protein Data Bank (PDB) ID code 1uwh] was selected for binding studies because it contains the DFG motif of the activation loop in the desirable inactive state (i.e., DFG-out). A homology model of PDGFRβ was created with a structurally related family member (VEGFR2; PDB ID code 1y6b). Further docking studies are provided in Fig. S1*B* and described in *SI Results*. (*B*) Human VSMCs were pretreated with **6** (0, 0.5, 1, and 10 μM) for 1 h followed by 7-min stimulation with PDGF-BB and lysis in RIPA buffer. Immunoprecipitation and immunoblotting were performed as described in *SI Materials and Methods*. To measure autophosphorylation, immunoblots were carried out with a phospho-tyrosine antibody. Membranes were stripped and reprobed for total PDGFRβ levels. (*C*) Western analysis demonstrating **6** (5 μM) inhibition of bFGF or VEGF (50 ng/mL, 5-min stimulation) induced phosphorylation of MEK and ERK in serum-starved HUVECs as described in *SI Materials and Methods*. A comparison of endothelial-cell-based RAF inhibition of **3** and **6** can be found in Fig. S2*A*. (*D*) Structure–activity relationships of the amino-triazole-based small molecules comparing both PDGFRβ and B-RAF. Compounds **3**–**11** were synthesized as described in Scheme 1 in *SI Materials and Methods* and screened for inhibition of PDGF-BB-induced PDGFRβ autophosphorylation in VSMCs at 2 μM (as described in *B*) or bFGF-induced MAPK activity in HUVECs at 5 μM by western analysis (as described in *C*) (–, x < 10%; +, 50% < x < 70%; + +, x > 90% inhibition). A full description of the SAR and important substituents can be found in *SI Results*. (*E* and *F*) XTT viability assay in which VSMCs (*E*) or HUVECs (*F*) were treated with **3**, **6**, imatinib, or sorafenib at various doses for 72 h in full growth medium containing 10% FBS as described in *SI Materials and Methods*. Curves represent the average of three separate experiments; error bars represent ± SEM.

Effect of Compounds on Cell Viability. We tested the effects of **3** versus **6** on VSMC or EC viability, because compound **3** inhibited PDGFRβ whereas compound **6** inhibited both RAF and PDGFRβ (see SARs in Fig. 1*D*). Compound **6** inhibited VSMC viability with an EC_{50} of 0.59 μM, whereas **3** produced an EC_{50} of 15.0 μM (Fig. 1*E*). Imatinib (PDGFRβ among its kinase targets) did not demonstrate any inhibition of VSMC viability at the highest concentration tested (20 μM). Compound **6** inhibited endothelial cell viability with an EC_{50} of 0.54 μM whereas **3** produced an EC_{50} of 18.04 μM (Fig. 1*F*), confirming our SAR demonstrating that the methylthiol group and both PDGFRβ and p-MEK inhibitory activity are critical for the cytotoxic effects observed. Interestingly, sorafenib, a RAF inhibitor with both type II and ATP competitive binding properties, produced an EC_{50} of 13.24 μM on the viability of the HUVECs, indicating that sorafenib was 25-fold less potent than **6** in this cell-based assay.

Compound 6 Interacts with PDGFR, a Type III Receptor Tyrosine Kinase, in Vitro. We further compared **6** to sorafenib in a panel of in vitro ATP-dependent kinase assays consisting of several targets that are inhibited by sorafenib. As expected for a pure type II inhibitor, **6** did not inhibit any of the following active kinases: B-RAF, C-RAF, VEGFR1, VEGFR2, Flt3, KIT, and PDGFRβ as well as several others, even at 10 μM (Table S1). This is not surprising given that **6** requires the inactive conformation of the enzyme for interaction. In contrast, sorafenib inhibits the kinase activity of B- and C-RAF in addition to VEGFR2 and several other receptor tyrosine kinases whereas **3**, like **6**, did not inhibit any of the active kinases tested.

We next analyzed **6** in a competitive binding assay (18) against 70 kinases (with the majority as inactive) representing diverse family members of the kinome (Fig. 2 and Table S2). Relative to other type II inhibitors imatinib and sorafenib, **6** displays improved selectivity, which is represented in the kinase dendrograms (Fig. 2). Among kinases, compound **6** inhibited only PDGFRα and β with K_ds of 300 and 520 nM, respectively, as well as Flt3 and KIT at 52 and 170 nM, respectively (Table S3). A panel of cyclin-dependent kinases (CDKs) was tested and weak binding was observed with CDKL2 (5.1 μM) and CDK11 (7.5 μM). Compound **6** did not inhibit RAF in this assay, but this is not surprising because the RAF construct used in this assay has an N-terminal regulatory domain truncation likely influencing the allosteric conformation.

Targeting RAF and PDGFR Activity in Cells. Although compound **6** failed to inhibit truncated RAF in the competitive binding assay, it completely disrupted phosphorylation of ERK T202/Y204 in cells expressing the constitutively active mutant of B-RAF (V600E), providing support that **6** directly targets RAF in cells (Fig. S2*B*). Additionally, **6** did not inhibit activation of either FGFR1 or VEGFR2 in endothelial cells (Fig. S2*E*) or in vitro (Table S2), but did inhibit the activation of PDGFRβ in SMCs (Fig. 1*B* and Fig. S2*E*). A summary of the phospho-sites examined in bFGF- or VEGFA-stimulated ECs is found in Table S4.

The specificity of **6** for RAF was further analyzed by evaluating its effect on specific phosphorylation sites both within and outside the RAF activation domain. Both bFGF and VEGF lead to phosphorylation of serine 338 (via PAK) within the activation domain of C-RAF, whereas serine 259, which mediates the coupling of C-RAF to the adaptor protein 14-3-3 (19), is constitutively phosphorylated (Fig. S2*C*). Compound **6** selectively blocked S338 phosphorylation, yet did not influence S259 (Fig. S2*C*), suggesting that its interaction with RAF preferentially influences its activation domain. Impor-

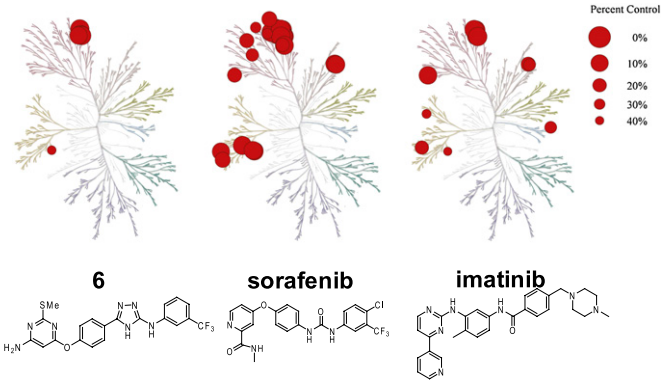

Fig. 2. Compound **6** demonstrates enhanced selectivity in kinome profiling. The profiles of **6**, sorafenib, and imatinib in the KINOME*scan* profiling service from Ambit Biosciences are shown. The compounds were screened against 70 kinases for competitive binding, and the legend describes % control (inhibition relative to positive control) of the kinase targets at 10 μM. The complete list of kinases screened as well as % inhibition are available in Table S2, and a list of the K_ds of the kinase targets for **6** can be found in Table S3. Kinome profiles for sorafenib and imatinib were reproduced with permission from Ambit Biosciences and have been previously reported (18).

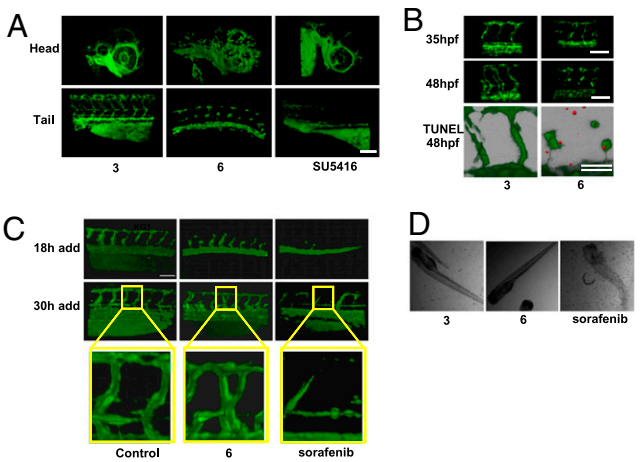

Fig. 3. Compound **6** inhibits angiogenesis in the zebrafish. (*A*) Effect of **6** on angiogenesis in transgenic *fli1-egfp* zebrafish embryos. Embryos were treated with 1 μM **6** or SU5416, or 10 μM **3** from 20 until 48 hpf. Representative 3D reconstructions of the blood vasculature are shown for both the head and tail regions of the embryo. Designations for the major vessels in the head and tail of the zebrafish embryo at 48 hpf are available in Fig. S3*A*. (*B*) Disruption of lumen formation in the zebrafish during late vessel maturation. Zebrafish treated with either 1 μM **6** or 10 μM **3** from 20 to 48 hpf were imaged at 35 and 48 hpf. (*Bottom*) **6** induces apoptosis in the intersegmental vessels in the zebrafish. Shown is a 3D overlap reconstruction of the GFP-expressing intersegmental vessels with TUNEL-positive nuclei at 48 hpf (shown in red). Representative phase-contrast views as well as quantification of intersegmental vessel volumes from *A* and *B* can be found in Fig. S3 *B–D*, respectively. (*C*) Time course of drug addition to zebrafish. Compounds (2.5 μM **3** or **6**, 1 μM sorafenib, or DMSO as control) were added at either 18 or 30 hpf (left on the embryos for the duration of the experiment), and intersegmental vessels were imaged ≈24 h after the time point corresponding to drug addition. At 30 hpf, the zebrafish embryos established early vessels with evident lumens. Compound **6** and sorafenib were added to evaluate their effect on preexisting vasculature. (*D*) Phase-contrast images of zebrafish treated with **3**, **6**, or sorafenib (same concentrations as in *C*). The images demonstrate that embryos treated with **3** and **6** are viable whereas sorafenib causes death. n = 4–6 zebrafish embryos per condition for all treatments. (Scale bars, 100 μm.)

tantly, **6** did not inhibit PAK, as it did not block PAK-mediated phosphorylation on MEK S298 in these cells (Fig. 1*C*).

Recent studies demonstrate the importance of B-RAF/C-RAF heterodimerization for effective MAPK signaling as heterodimerization dramatically increases the activity of both B-RAF and C-RAF (20, 21). Furthermore, certain mutations which induce an "open conformation" of B-RAF promote constitutive binding to C-RAF in cancer cells, and this heterodimerization activates C-RAF and MEK signaling (22). This defines RAF heterodimerization as an intriguing target for disrupting RAF activity in cells. To evaluate the effect of compound **6** on RAF heterodimerization, we induced endogenous RAF heterodimerization in ECs by stimulating the cells with bFGF or VEGF and studied the ability of **6** to impact the formation of this complex (Fig. S2*D*). Treatment of cells with **6** completely inhibited this heterodimer formation as well as ERK phosphorylation in response to either growth factor, whereas **3** had no effect (Fig. S2*D*). Interestingly, a MEK inhibitor, U0126, inhibited phosphorylation of ERK as expected, but greatly increased RAF heterodimerization above that achieved with growth-factor stimulation alone, suggesting the possibility of a feedback loop upon MEK inhibition. The finding that **6** inhibits phosphorylation of MEK and ERK in endothelial cells stimulated with bFGF or VEGF (Fig. 1*C*) provides evidence that **6** targets both B-RAF and C-RAF in cells, and inhibition of MAPK signaling by disrupting RAF heterodimerization may be an ideal mechanism to deal with the compensatory roles of B-RAF and C-RAF.

Compound 6 Disrupts a Late Step in Angiogenesis During Zebrafish Embryogenesis. Although originally selected for antiangiogenic activity in zebrafish, the effects of **6** were further analyzed in this model to assess its mechanistic impact on new blood vessel growth. In embryos treated with **6** (1 μM in water), endothelial cells migrated away from the dorsal aorta as typically observed in control animals, yet by 48 hpf they failed to form mature intersegmental vessels and similarly impacted the developing vasculature within the head region (Fig. 3*A*), whereas **3**, which inhibits PDGFRβ but not B-RAF, had no effect. Following treatment, the blood vessels appeared highly disorganized and lacked the capacity to support blood flow. In contrast, fish treated with **3**, even up to 10 μM, were indistinguishable from nontreated controls (Fig. 3*A*). Labeling of the major vascular structures, phase contrast views of the embryos, and quantification of the intersegmental vessel volumes are available in Fig. S3 *A–D*. It is important to note that compound **3** has K_ds of 1.4, 3.7, 32, and 40 nM against Flt3, KIT, PDGFRα, and PDGFRβ, respectively, in the competitive binding assay used in Fig. 2. Because compound **3** is ineffective at inhibiting angiogenesis in the zebrafish developmental embryogenesis model, it is clear that Flt3 and KIT do not play a role in blood vessel formation. Interestingly, SU5416 (**12**), a VEGFR2 inhibitor, although completely disrupting endothelial cell migration and neovascularization in the tail, had minimal effects on ocular vessels in these animals, suggesting that VEGF does not play an important role during ocular vascular development.

To analyze the temporal effects of **6** on angiogenesis, zebrafish were treated with **6** at 18 hpf and then analyzed at 35 hpf as lumens were beginning to form. Interestingly, **6** showed no apparent effect on the vessels at 35 hpf, whereas imaging at 48 hpf suggests **6** impacts a late step in lumen formation (Fig. 3*B*). This was followed by the induction of apoptosis as shown by TUNEL-stained intersegmental ECs at 48 hpf (Fig. 3*B*). In contrast, addition of **6** at 30 hpf (at the time when intersegmental vessel structure is first established) did not suppress vascular growth and patterning (Fig. 3*C*), suggesting that once lumen formation is initiated, neovessels in these animals are resistant to the effect of **6**. In contrast, sorafenib not only prevented the formation of new blood vessels but also disrupted mature intersegmental blood vessels when added at 30 hpf (Fig. 3*C*). Additionally, treatment of embryos with **6** at 48–72 hpf had no effect on mature intersegmental vessels and the zebrafish were all viable, whereas treatment with sorafenib at this late time point induced death in all animals tested (Fig. 3*D*). Thus, **6** appears to disrupt a late step in neovascularization without

detectable toxicity, whereas sorafenib suppresses multiple processes during embryogenesis, leading to lethality.

Dual Inhibition of PDGFRβ and RAF Is Required to Produce the Antiangiogenic Effect. The requirement for dual inhibition of PDGFRβ and RAF for angiogenesis inhibition was investigated in the zebrafish model. Only the combination of RAF inhibition (GW 5074, **13**) and PDGFRβ inhibition (imatinib) led to a similar phenotype to **6,** in which angioblasts migrate from the dorsal aorta and posterior cardinal vein but fail to form functional vessels with open lumens capable of supporting blood flow (Fig. 4*A*). Representative images of Tg:*fli1-EGFP* zebrafish embryos demonstrate that 5 μM imatinib or 1 μM GW 5074 do not have an effect on intersegmental vessel formation, and functional vessels with open lumens are observed (Fig. 4*A*).

To validate these findings, we used a coculture angiogenesis assay to evaluate similar combinations of PDGFR and RAF inhibitors. In this assay, human umbilical vein endothelial cells (HUVECs) are mixed with hepatic stellate cells (a pericyte found in the perisinusoidal space of the liver) in a 3D collagen gel. The coculture produces endothelial tubes with pericyte contacts (from the stellate cells) that can be imaged and quantified as shown in Fig. 4 *B* and *C*. Treatment of the cocultures with 2.5 μM **6** leads to a dramatic reduction in both overall endothelial tube formation as well as % pericyte-covered tube length (Fig. 4 *B* and *C*). Addition of 2.5 μM **3** or 1.0 μM imatinib, which are both PDGFRβ inhibitors, does not affect endothelial tube formation or cause a significant change in pericyte coverage of the endothelial tubes (Fig. 4 *B* and *C*). Importantly, a previously identified RAF inhibitor, GW 5074, did not affect pericyte coverage or tube length alone, but combination with 1.0 μM imatinib produced a similar decrease in the % pericyte-covered tube length compared to **6** (Fig. 4 *B* and *C*).

Compound 6 Blocks Angiogenesis and Inhibits RAF/PDGFRβ in Mice. To assess the antiangiogenic properties of **6** in a mammalian model, mice were s.c. injected with Matrigel containing bFGF to induce neovascularization and systemically treated with **6** at 50 mg/kg, i.p., bid (twice daily) (pharmacokinetic analysis of the dose and formulation of **6** used indicated a C_{max} of 3.6 μg/mL or 7.7 μM, $T_{1/2}$ corresponding to 11.5 h, and an area under the concentration time curve ($AUC^{0–12h}$) of 14.7 μg·h/mL). At this dose, **6** completely blocked angiogenesis relative to vehicle control (Fig. S4*A*). To monitor the effects of **6** on RAF signaling in vivo, we evaluated cryosections of bFGF-stimulated tissues for the presence of p-ERK immunostaining. bFGF stimulation of these tissues led to intense p-ERK staining in both invasive endothelial and stromal cells. Systemic treatment of animals with **6** blocked MAPK pathway signaling within endothelial cells, as we observed suppression in p-ERK staining in these cells (Fig. S4*B*). Additionally, vehicle-treated mice displayed intense p-PDGFRβ Y751 in smooth muscle actin-positive cells (Fig. S4*C*), whereas mice treated with **6** demonstrated a complete suppression in the p-PDGFRβ Y751 signal associated with the stromal compartment surrounding endothelial cells (Fig. S4*C*). We observed intense TUNEL staining among the neovessels in these tissues but much less staining associated with the stromal cells adjacent to these vessels (Fig. S4*D*). Therefore, **6** disrupts a survival signal in actively growing blood vessels.

Compound 6 Prevents Tumor Growth in an Orthotopic Pancreatic Carcinoma Model. We next examined the effect of **6** on the growth and angiogenic response of an orthotopic XPA-1 pancreatic carcinoma model. Animals were systemically treated with either vehicle or **6** (50 mg/kg, bid) beginning 3 days after surgical orthotopic implantation (SOI) of a tumor fragment. Tumor growth was monitored noninvasively by whole-body imaging. Tumor growth was completely suppressed in animals treated with **6** compared to vehicle alone 12 days post-SOI. Representative time-course images (lateral view) from three animals demonstrate that the growth of

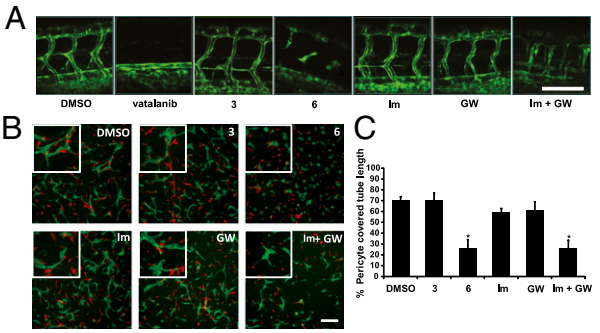

Fig. 4. Combination of imatinib and GW 5074 inhibits angiogenesis similarly to compound **6**. (*A*) Effect of **3**, **6**, vatalanib, imatinib, GW 5074, and a combination of imatinib (PDGFR inhibitor) and GW 5074 (RAF inhibitor) on intersegmental vessel formation in Tg:(*fli1-egfp*) zebrafish embryos. Embryos were treated with DMSO, 5 μM **3**, 5 μM **6**, 1 μM vatalanib, 5 μM imatinib (Im), 1 μM GW 5074 (GW), and the combination of 5 μM imatinib and 1 μM GW 5074 (Im + GW) from 16 until 48 hpf. Z stacks from laser-scanning confocal microscopy are shown depicting formation of the intersegmental vessels at 48 hpf. $n = 6$ embryos/treatment. (Scale bar, 100 μm.) (*B*) HUVECs were cocultured with hTERT-human hepatic stellate cells in a 3D collagen matrix in the presence of complete EBM-2 medium to monitor pericyte-associated endothelial tube formation. The stellate cells were labeled with 10 μg/mL red fluorescent dye [DiIC(3); BD Biosciences] for 1 h before the start of the experiment. Inhibitors were added to the cocultures 6 h postseeding at the following concentrations: DMSO, 2.5 μM **3**, 2.5 μM **6**, 1 μM imatinib (Im), 0.5 μM GW 5074 (GW), and the combination of 1 μM imatinib and 0.5 μM GW 5074 (Im + GW). The endothelial tubes were stained at 24 h by adding 2 μL FITC-labeled *Ulex europaeus* lectin (Vector Labs) per well. Images were acquired 48 h postseeding of the cells. One representative panel from three independent experiments is shown. Green, FITC-lectin-labeled endothelial cells; red, DiIC(3)-labeled stellate cells. Inset in each panel displays a higher-magnification view of the endothelial cell/stellate cell interactions. (Scale bar, 200 μm.) (*C*) Tube lengths were measured using MetaMorph software for each tube for all 10 fields that were acquired. The % pericyte-covered tube length was calculated from the ratio of tube length sums for the tubes with and without pericyte contact. Error bars are reported as ± SEM of two wells per group. $^*P < 0.05$ compared to DMSO group.

pancreatic tumors treated with **6** was suppressed and RFP intensity was abolished by day 12 after SOI compared to vehicle-treated animals (Fig. 5*A*). Clearly, **6** suppressed tumor growth in this model (Fig. 5*B*) but caused no weight loss (Fig. 5*C*), and the mice did not demonstrate any signs of lethargy. Animals treated with **6** produced an average tumor weight of 26.7 mg compared to 74.1 mg for vehicle-treated animals (Fig. 5*D*). At this time, GFP-labeled blood vessels were imaged and tumor-associated blood vessel density was quantified by measuring the ratio of total blood vessel length to tumor volume (Fig. 5 *E* and *F*). Tumors treated with **6** were substantially less vascularized relative to vehicle treatment, and images of the GFP-labeled tumor vasculature showed a significant reduction in the total blood vessels present (Fig. 5*E*). The mean vessel length/tumor volume was 2.5 mm/mm^3 compared to 0.2 mm/mm^3 for vehicle and **6**, respectively (Fig. 5*F*).

Compound 6 Prevents Tumor Growth in an Orthotopic Renal Cell Carcinoma Model After Oral Administration. To test the effects of **6** on tumor growth after oral administration, human SN12C renal cells expressing RFP were injected into the kidney capsule of nude mice and tumors were allowed to develop for 7 days. Compound **6** was dosed at 100 mg/kg and demonstrated favorable pharmacokinetics with a C_{max} of 4.9 μg/mL, $T_{1/2}$ of 6.1 h, and an $AUC^{0–24h}$ of 8.7 μg·h/mL. Suppression of tumor growth was readily observed in those animals treated with **6** (Fig. S5*A*). On day 26, the kidneys were excised from these animals and the weight due to tumor was calculated by subtracting the weight of the normal kidney from the weight of the tumor-bearing kidney for each animal. The average tumor burden of the vehicle group was 132 ± 39 mg compared to 49 ± 18 mg for the **6**-treated group

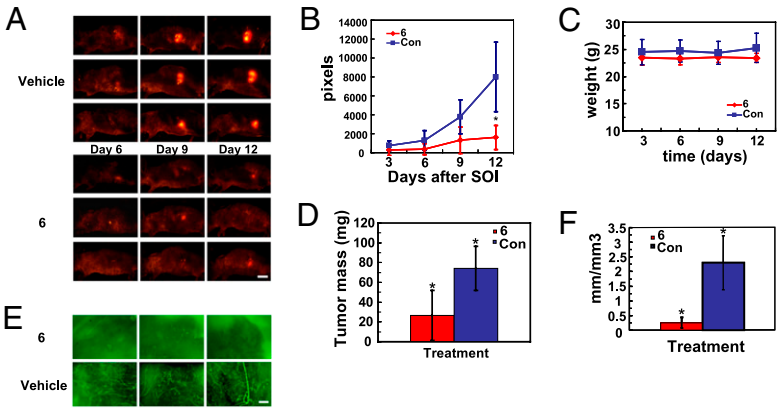

Fig. 5. Compound **6** inhibits pancreatic tumor growth and reduces tumor vascular density. (*A*) Real-time fluorescent imaging of XPA-1-RFP pancreatic tumor xenografts in the pancreas of Nestin-GFP mice (n = 5/group) treated with either vehicle or **6** (50 mg/kg, i.p., bid). Drug treatments were started 3 days after surgical orthotopic implantation (SOI) of XPA-1-RFP tumors, and tumor progression was monitored every 3 days by whole-animal imaging. (Scale bar, 10 mm.) (*B*) Plot of tumor surface area over time for the vehicle- and **6**-treated groups. Tumor surface area was calculated by adding the total pixels of both the ventral and lateral images of the tumor. *P = 0.034. (*C*) Average body weight of the mice measured each day of whole-animal imaging described in *A* and *B*. (*D*) Total weights of resected primary tumors on day 15 post-SOI. *P = 0.022. (*E*) Representative fluorescent images of endothelial GFP expression (GFP expression driven by the Nestin promoter) within the XPA-1-RFP tumors after resection. Images were taken 15 days post-SOI. (Scale bar, 200 μm.) (*F*) Plot of tumor vessel density from images acquired as in *E*. Blood vessels imaged as in *E* were converted to length (mm) and normalized to tumor volume (mm^3). *P = 0.01.

(Fig. S5*B*). This demonstrates the oral activity of **6** in preventing tumor growth of an orthotopic renal cell carcinoma model.

Discussion

Type II inhibitors represent a new paradigm for drug selection as seen with the cocrystal structures of Abl with imatinib and B-RAF with sorafenib (16, 17). The first inactive conformation was observed in the crystal structure of the insulin receptor, and at least nine compounds have now been shown to interact with the allosteric site in various kinases (13). This relatively new approach of stabilizing the inactive kinase conformation has led to the development of novel inhibitors which stabilize the DFG-out conformation, and are the subject of recent reviews (13, 14). Due to the hydrophobic interactions and specific hydrogen bonding required for type II inhibition, the allosteric site adjacent to the kinase active site may be used to improve specificity over the type I inhibitors that interact solely with the active kinase conformation in the highly conserved hinge region. Lapatinib, a small molecule that targets the inactive state of EGFR, highlights this potential selectivity advantage of stabilizing the inactive state, because it represents one of the most selective kinase inhibitors currently known and has a slow dissociation rate similar to type II inhibitors (23).

Based on our rational design approach coupled with cell-based screening directly in the primary cell types relevant to angiogenesis, ECs and VSMCs, we identified compounds that potently inhibit RAF and PDGFR and thereby block angiogenesis and tumor growth in vivo. Importantly, this molecule, **6**, would have been disregarded using traditional in vitro ATP-dependent kinase assays, as 10 μM **6** did not inhibit any of its targets in this screening format (Table S1). For PDGFRβ, the cellular IC_{50} and biochemical K_d matched quite well as both were ≈500 nM (Fig. 1*B* and Table S3), demonstrating a significant difference between the activity of **6** in cell-based versus activated-kinase assays. This is perhaps not surprising, because the recombinant enzymes are not subject to the same conformational inactivation as the intact cell-associated enzymes. Although **6** is predicted to stabilize the inactive conformation of PDGFRβ or B-RAF, it might not be expected to suppress the activity of recombinant activated forms of these enzymes in vitro that are not subject to negative regulation. Similarly, imatinib, a known type II kinase inhibitor, is 200-fold more active against the Abl kinase domain when the activation loop is unphosphorylated (17).

Whereas **6** inhibited cellular PDGFR and RAF, it also disrupted Flt3 and KIT (Table S3). However, Flt3 and KIT were not essential to the biological activity of **6** because compound **3**, which blocks Flt3, KIT, and PDGFR but does not inhibit RAF, failed to disrupt vessel formation (Fig. 3 *A* and *B*). This result further supports the synergy of inhibiting both PDGFR and RAF for increased antiangiogenic activity, as observed in Fig. 4 using completely different chemotypes.

The stromal compartment is now recognized as a major contributor to angiogenesis and tumor growth (24, 25). This includes pericytes associated with the newly forming endothelium, which stabilize the vasculature and promote vascularization (26). PDGFRβ signaling potentiates pericyte recruitment to newly forming vessels and the secretion of proangiogenic molecules such as VEGFA, FGF2, and Ang1 in the local microenvironment. This promotes vessel stabilization and remodeling of the immature vascular network to a highly ordered network (27–29). Maintenance of the vascular compartment is dependent upon paracrine loops such as the secretion of PDGF-BB and FGF2, which lead to increased expression of FGFR1 on VSMCs and PDGFRα/β on ECs, respectively (28). Therefore, the homeostasis of the mural and vascular compartments is critical for efficient angiogenesis. We rationalized that inhibiting these two compartments simultaneously would initiate a potent inhibition of angiogenesis. Although broad-spectrum receptor tyrosine kinase inhibitors are available, our goal was to design compounds with a narrow kinase profile to selectively inhibit relevant pathways involved in neovascularization. We targeted RAF kinase because this kinase is known to be downstream of multiple receptor tyrosine kinases and is required for EC proliferation and survival (1), and PDGFRβ, which is known to be critical for pericyte recruitment and vessel maturation. Fortunately, the PDGFRβ and B-RAF allosteric sites are quite similar, enabling an effort to develop selective inhibitors of these two targets (Fig. 1*A*).

Here we report the development of selective inhibitors directed against PDGFRβ and RAF, and define a synergistic combination which leads to effective inhibition of angiogenesis and tumor growth. Although new clinically approved kinase inhibitors work through broad-spectrum inhibition and opportune target combinations, we define a strategy to narrow the kinase profile to selective combinations which provide great synergy. This approach will ultimately increase the therapeutic window of these agents and improve the chance of providing therapeutic efficacy with minimal side effects.

Materials and Methods

Animal Studies. All animal procedures were conducted in accordance with all appropriate regulatory standards under protocols S05018 and S06008 approved by the UCSD Institutional Animal Care and Use Committee.

Computational Docking Studies and Chemical Synthesis. The molecular modeling and homology model of PDGFRβ are described in *SI Materials and Methods*. All compounds were synthesized from commercially available starting materials, and schemes, synthetic procedures, and purification details are available in *SI Materials and Methods*.

In Vitro Kinase Screen and Competitive Binding Assay. Sorafenib as well as test compounds were submitted to Invitrogen and screened using their SelectScreen profiling service. For the competitive binding assay, test compounds were screened at 10 μM against 70 diverse kinase targets for competitive binding

using KINOME*scan* technology (Ambit Biosciences) (18). Eleven-point K_d curves were determined for hits identified during the initial screen.

Cell Culture and Cell-Based Screening. HUVECs and VSMCs (Lonza) were maintained as recommended, with all experiments conducted at passage <6. XPA-1-RFP and SN12C-RFP cells were maintained under standard culture conditions in RPMI supplemented with 10% FBS. XPA-1 cells were a gift from Dr. Anirban Maitra (Baltimore, MD) and transduced with retrovirus to establish stable RFP-expressing cells as described previously (30). For cell-based assays, subconfluent cells were starved overnight in serum-free medium, pretreated with inhibitor, and stimulated with growth factor as described in the figure legends. A description of the immunoprecipitation, immunoblotting, and antibodies is available in *SI Materials and Methods*.

Zebrafish Studies. Transgenic Tg(*fli1:EGFP*) zebrafish embryos were purchased from the Zebrafish Model Organism Database (http://www.zfin.org) and reported elsewhere (31) and maintained as previously described (32). Compounds in DMSO stock solutions were diluted directly into water and vessels were imaged for GFP expression using a Nikon c1-si confocal microscope. Apoptosis was measured by TUNEL staining using the Apoptag in situ red fluorescence kit (Chemicon) with a protocol described previously (33).

Stellate Cell/Endothelial Cell Tube Formation Assay and Mouse Matrigel Model. This assay was performed as described in *SI Materials and Methods*. The stellate cells were a gift from Dr. David Brenner (La Jolla, CA) and previously described (34). The 3D collagen assay for tube formation was performed as previously described (35). The mouse Matrigel model was performed as previously described (36), and further details of immunohistochemistry and animal dosing can be found in *SI Materials and Methods*.

Orthotopic Pancreatic Carcinoma and Renal Cell Carcinoma Models. Six-week-old male Nestin-GFP nude mice described previously (37, 38) underwent surgical orthotopic implantation of XPA-1-RFP pancreatic tumor cells as described previously (39, 40) and in further detail in *SI Materials and Methods*. The renal cell carcinoma model was used as previously described (41), and is given in further detail in *SI Materials and Methods*.

Statistical Calculations. All statistical evaluation was done using NCSS 2007 statistical software. For comparisons between two groups, a two-tailed *t* test was used for data with equal variance and the Aspin–Welch unequal variance test was used for data with unequal variance. For comparison between more than two groups a one-way ANOVA was used. *P* values are noted in the figure legends.

Note Added in Proof. Two recent studies report RAF inhibitors inducing BRAF binding to CRAF in Ras mutant or Ras/RAF wild-type cells, leading to CRAF activation and tumor progression (42, 43). Importantly, these studies warn against the use of ATP-competitive BRAF inhibitors since they act as either inhibitors or activators of signaling pathways, depending on the cellular context and suggest the development of allosteric, non-ATP competitive RAF inhibitors that prevent RAF dimerization (43). Compound **6** was designed to stabilize the inactive state of RAF without competing with ATP and shown to disrupt BRAF/CRAF heterodimerization in Fig. S2*D*. Importantly, specific tumor cell lines which were activated with ATP-competitive RAF inhibitors (43) were suppressed with compound **6**.

ACKNOWLEDGMENTS. This work was supported by grants from the NIH: P01-CA078045 (to D.A.C.), P01-HL057900 (to D.A.C.), and P01-CA104898 (to D.A.C.). We thank Leo Barnes for his assistance with animal studies. We also thank Brad Larson and Ryan Fischer for performing the Invitrogen SelectScreen kinase assay panel. We thank Dr. David Brenner for supplying the hTERT stellate cells used in the coculture endothelial tube formation assay.

1. Alavi A, Hood JD, Frausto R, Stupack DG, Cheresh DA (2003) Role of Raf in vascular protection from distinct apoptotic stimuli. *Science* 301:94–96.
2. Hood JD, et al. (2002) Tumor regression by targeted gene delivery to the neovasculature. *Science* 296:2404–2407.
3. Danis R, et al. (2003) Intravitreous anti-raf-1 kinase antisense oligonucleotide as an angioinhibitory agent in porcine preretinal neovascularization. *Curr Eye Res* 26:45–54.
4. Andrae J, Gallini R, Betsholtz C (2008) Role of platelet-derived growth factors in physiology and medicine. *Genes Dev* 22:1276–1312.
5. Abramsson A, Lindblom P, Betsholtz C (2003) Endothelial and nonendothelial sources of PDGF-B regulate pericyte recruitment and influence vascular pattern formation in tumors. *J Clin Invest* 112:1142–1151.
6. Jain RK (2003) Molecular regulation of vessel maturation. *Nat Med* 9:685–693.
7. Druker BJ, et al.; IRIS Investigators (2006) Five-year follow-up of patients receiving imatinib for chronic myeloid leukemia. *N Engl J Med* 355:2408–2417.
8. Druker BJ, et al. (2001) Efficacy and safety of a specific inhibitor of the BCR-ABL tyrosine kinase in chronic myeloid leukemia. *N Engl J Med* 344:1031–1037.
9. Wilhelm S, et al. (2006) Discovery and development of sorafenib: A multikinase inhibitor for treating cancer. *Nat Rev Drug Discov* 5:835–844.
10. Druker BJ, et al. (1996) Effects of a selective inhibitor of the Abl tyrosine kinase on the growth of Bcr-Abl positive cells. *Nat Med* 2:561–566.
11. Lyons JF, Wilhelm S, Hibner B, Bollag G (2001) Discovery of a novel Raf kinase inhibitor. *Endocr Relat Cancer* 8:219–225.
12. Wilhelm SM, et al. (2004) BAY 43-9006 exhibits broad spectrum oral antitumor activity and targets the RAF/MEK/ERK pathway and receptor tyrosine kinases involved in tumor progression and angiogenesis. *Cancer Res* 64:7099–7109.
13. Liu Y, Gray NS (2006) Rational design of inhibitors that bind to inactive kinase conformations. *Nat Chem Biol* 2:358–364.
14. Okram B, et al. (2006) A general strategy for creating "inactive-conformation" Abl inhibitors. *Chem Biol* 13:779–786.
15. Pargellis C, et al. (2002) Inhibition of p38 MAP kinase by utilizing a novel allosteric binding site. *Nat Struct Biol* 9:268–272.
16. Wan PT, et al.; Cancer Genome Project (2004) Mechanism of activation of the RAF-ERK signaling pathway by oncogenic mutations of B-RAF. *Cell* 116:855–867.
17. Schindler T, et al. (2000) Structural mechanism for STI-571 inhibition of Abelson tyrosine kinase. *Science* 289:1938–1942.
18. Karaman MW, et al. (2008) A quantitative analysis of kinase inhibitor selectivity. *Nat Biotechnol* 26:127–132.
19. Rommel C, et al. (1996) Activated Ras displaces 14-3-3 protein from the amino terminus of c-Raf-1. *Oncogene* 12:609–619.
20. Rushworth LK, Hindley AD, O'Neill E, Kolch W (2006) Regulation and role of Raf-1/B-Raf heterodimerization. *Mol Cell Biol* 26:2262–2272.
21. Weber CK, Slupsky JR, Kalmes HA, Rapp UR (2001) Active Ras induces heterodimerization of cRaf and BRaf. *Cancer Res* 61:3595–3598.
22. Garnett MJ, Rana S, Paterson H, Barford D, Marais R (2005) Wild-type and mutant B-RAF activate C-RAF through distinct mechanisms involving heterodimerization. *Mol Cell* 20:963–969.
23. Wood ER, et al. (2004) A unique structure for epidermal growth factor receptor bound to GW572016 (Lapatinib): Relationships among protein conformation, inhibitor off-rate, and receptor activity in tumor cells. *Cancer Res* 64:6652–6659.
24. Jung YD, et al. (2002) The role of the microenvironment and intercellular cross-talk in tumor angiogenesis. *Semin Cancer Biol* 12:105–112.
25. Nyberg P, Salo T, Kalluri R (2008) Tumor microenvironment and angiogenesis. *Front Biosci* 13:6537–6553.
26. von Tell D, Armulik A, Betsholtz C (2006) Pericytes and vascular stability. *Exp Cell Res* 312:623–629.
27. Uemura A, et al. (2002) Recombinant angiopoietin-1 restores higher-order architecture of growing blood vessels in mice in the absence of mural cells. *J Clin Invest* 110:1619–1628.
28. Nissen LJ, et al. (2007) Angiogenic factors FGF2 and PDGF-BB synergistically promote murine tumor neovascularization and metastasis. *J Clin Invest* 117:2766–2777.
29. Pietras K, Pahler J, Bergers G, Hanahan D (2008) Functions of paracrine PDGF signaling in the proangiogenic tumor stroma revealed by pharmacological targeting. *PLoS Med* 5:e19.
30. Tsuji K, et al. (2006) Common bile duct injection as a novel method for establishing red fluorescent protein (RFP)-expressing human pancreatic cancer in nude mice. *JOP* 7:193–199.
31. Lawson ND, Weinstein BM (2002) In vivo imaging of embryonic vascular development using transgenic zebrafish. *Dev Biol* 248:307–318.
32. Brand M, Granato M, Nusslein-Volhard C (2002) in *Zebrafish: A Practical Approach,* eds Nusslein-Volhard C, Dahm R (Oxford University Press, New York), pp 7–38.
33. Stanton SE, McReynolds LJ, Evans T, Schreiber-Agus N (2006) Yaf2 inhibits caspase 8-mediated apoptosis and regulates cell survival during zebrafish embryogenesis. *J Biol Chem* 281:28782–28793.
34. Schnabl B, Choi YH, Olsen JC, Hagedorn CH, Brenner DA (2002) Immortal activated human hepatic stellate cells generated by ectopic telomerase expression. *Lab Invest* 82:323–333.
35. Koh W, Stratman AN, Sacharidou A, Davis GE (2008) In vitro three dimensional collagen matrix models of endothelial lumen formation during vasculogenesis and angiogenesis. *Methods Enzymol* 443:83–101.
36. Eliceiri BP, et al. (1999) Selective requirement for Src kinases during VEGF-induced angiogenesis and vascular permeability. *Mol Cell* 4:915–924.
37. Amoh Y, et al. (2005) Nestin-linked green fluorescent protein transgenic nude mouse for imaging human tumor angiogenesis. *Cancer Res* 65:5352–5357.
38. Amoh Y, et al. (2006) Dual-color imaging of nascent blood vessels vascularizing pancreatic cancer in an orthotopic model demonstrates antiangiogenesis efficacy of gemcitabine. *J Surg Res* 132:164–169.
39. Katz MH, et al. (2003) Selective antimetastatic activity of cytosine analog CS-682 in a red fluorescent protein orthotopic model of pancreatic cancer. *Cancer Res* 63:5521–5525.
40. Bouvet M, et al. (2002) Real-time optical imaging of primary tumor growth and multiple metastatic events in a pancreatic cancer orthotopic model. *Cancer Res* 62:1534–1540.
41. An Z, Jiang P, Wang X, Moossa AR, Hoffman RM (1999) Development of a high metastatic orthotopic model of human renal cell carcinoma in nude mice: Benefits of fragment implantation compared to cell-suspension injection. *Clin Exp Metastasis* 17: 265–270.
42. Heidorn SJ, et al. (2010) Kinase-dead BRAF and oncogenic RAS cooperate to drive tumor progression through CRAF. *Cell* 140:209–221.
43. Hatzivassiliou G, et al. (2010) RAF inhibitors prime wild-type RAF to activate the MAPK pathway and enhance growth. *Nature*, 10.1038/nature08833.